Spatial Control of the Hole Accumulation Zone for Hole-Dominated Perovskite Light-Emitting Diodes by Inserting a CsAc Layer

Zhu, Zhaohua; Li, Yang; Guan, Zhiqiang; Wu, Yan; Zeng, Zixin; Tsang, Sai-Wing; Liu, Shihao; Huang, Xiao; Lee, Chun-Sing

Published in:
ACS Applied Materials & Interfaces

Published: 08/02/2023

Document Version:
Post-print, also known as Accepted Author Manuscript, Peer-reviewed or Author Final version

Published version (DOI):
10.1021/acsami.2c19230

Publication details:
Zhu, Z., Li, Y., Guan, Z., Wu, Y., Zeng, Z., Tsang, S.-W., Liu, S., Huang, X., & Lee, C.-S. (2023). Spatial Control of the Hole Accumulation Zone for Hole-Dominated Perovskite Light-Emitting Diodes by Inserting a CsAc Layer. *ACS Applied Materials & Interfaces*, *15*(5), 7044–7052. https://doi.org/10.1021/acsami.2c19230

Spatial Control of Hole Accumulation Zone for Hole-Dominate Perovskite Light-Emitting Diodes by Inserting CsAc Layer

Zhaohua Zhu[12], Yang Li[12], Zhiqiang Guan[12], Yan Wu[12], Zixin Zeng[4], Sai-Wing Tsang[4], Shihao Liu[12], Xiao Huang[3*], Chun-Sing Lee[12*]*

1 Center of Super-Diamond and Advanced Films (COSDAF), City University of Hong Kong, Kowloon, Hong Kong SAR 999077, P. R. China

2 Department of Chemistry, City University of Hong Kong, Kowloon 999077, Hong Kong SAR, P. R. China

3 Institute of Advanced Materials (IAM), Nanjing Tech University, 30 South Puzhu Road, Nanjing, 211816 P. R. China

4 Department of Material Science and Engineering, City University of Hong Kong, Kowloon 999077, Hong Kong SAR, P. R. China

*Corresponding author

E-mail: liushihao@jlu.edu.cn, iamxhuang@njtech.edu.cn, apcslee@cityu.edu.hk

KEYWORDS perovskite, light-emitting diodes, charge balance, hole-blocking, charge accumulation

ABSTRACT

Perovskites show efficient electroluminescence and are expected to have wide applications in light-emitting diodes (LEDs). However, owing to the unbalanced electron–hole transport properties of some highly luminescent perovskites, a fundamental challenge is that the exciton recombination zone of perovskite LEDs (PeLEDs) typically overlaps with accumulation of the major carrier. It is known to reduce performances of PeLEDs, leading to reduction of efficiency and operation stability due to Auger recombination. To address this issue in a hole-dominate blue PeLED, we propose to insert a cesium acetate (CsAc) layer between hole transport layer (HTL) and the hole-dominant perovskite layer. Electronic properties indicate that hole accumulation zone of the device with the CsAc layer shifts away from the perovskite/ETL interface, i.e. the recombination zone, to the HTL/CsAc interface. Separation of the hole accumulation region and the exciton recombination zones substantially suppress exciton quenching. Moreover, the CsAc layer can also improves the photophysical properties of the perovskite film by providing extra Cs source to interact with defect site of unreacted $PbBr_2$ in the perovskite film and enhance the crystallinity of perovskite with enlarged crystal grain size. As a result, the external quantum efficiency (EQE) of the sky-blue PeLEDs show considerable improvement from 5.3 to 9.2% upon inserting the CsAc layer.

1. Introduction

Perovskite, as a promising class of semiconductor materials, have been widely adopted in light-emitting diodes (LEDs) due to its outstanding properties, such as good color purity, high photoluminescence quantum yield, color tunability, low cost and solution-processibility.[1-9] The external quantum efficiency (EQE) of perovskite light-emitting diodes (PeLEDs) have reached over 20% for near-infrared, red, and green lights.[10-13] However, the EQE of blue PeLEDs is still lagging behind, which hinders the practical applications of PeLEDs for full-color display and lighting.[14-20]

Similar to the case of organic light-emitting diodes (OLEDs), unbalance of electron and hole currents in PeLEDs would lead to non-radiative losses and thus decreased performance.[21,22] To achieve highly efficient PeLEDs, one of the effective ways is to improve charge balance by spatially confining the excitons or charge carriers inside the perovskite layer.[23] However, owing to the unbalanced electron and hole transporting properties of some highly luminescent perovskites, the majority carriers would accumulate at the interfaces between the perovskite layer and the carrier transport layer of the minority carrier. Typically, the hole mobility of perovskite is higher than its electron mobility.[24] This would result in hole accumulation at the perovskite/electron transport layer (ETL) interface.[25] Charge blocking layer has been adopted to reduce the major carrier transport rate to balance carriers injection.[26,27] For example, Zhang et al. inserted an additional polyvinyl pyrrolidone (PVP) buffer layer which block excess electrons injection into perovskite layer.[26] However, additional layer for blocking holes in PeLEDs have rarely been reported. On the other hand, spatial

distribution of excitons would also be influenced by the unbalanced transports of perovskites. Due to the attraction of the localized majority carriers, it is reasonably to consider that many excitons are formed at the interface where the majority carriers accumulate. It results in an overlap between the recombination zone and the carrier accumulation zone. In this case, energy released from the recombination of excitons would directly transfer to the majority carriers accumulated at the heterojunction through Auger recombination,[22] which is detrimental to the performance of PeLEDs.[28] Besides, the mismatch between hole mobility of hole transport layer (HTL) and electron mobility of the electron transport layer (ETL) could further aggravate the charge accumulation and the Auger recombination.[24] For instance, in a typical perovskite LEDs, poly(3,4-ethylenedioxythiophene) polystyrene sulfonate (PEDOT:PSS) and 2,2',2"-(1,3,5-Benzinetriyl)-tris(1-phenyl-1-H-benzimidazole) (TPBi) are respectively used as HTL and ETL.[29,30] It is known that the hole mobility of PEDOT:PSS is much higher than the electron mobility of TPBi.[31] Although electron transport materials with deep HOMO level, e.g. POT2T,[32] B3PYMPM[33] and so on, can act as hole blocking layer which can confine hole in the perovskite layer;[34,35] these still cannot avoid the accumulation of holes at the perovskite/ETL interface. In short, the important challenge is that the recombination zone of PeLEDs usually overlaps with accumulation zone of the major carrier, and this leads to serious non-radiative recombination losses. Although the carrier balance can be modulated, to some extent, by controlling the thicknesses of transport layers,[23] the device performances are still not maximized due to the intrinsic unbalanced transport properties of perovskite crystal.

In this work, a hole-dominant blue PeLED is first optimized by modulating the thickness of HTL. We then demonstrated that the optimized efficiency can be further enhanced by inserting an extra hole blocking cesium acetate (CsAc) layer between the perovskite and the HTL. A systemic investigation suggests that the CsAc layer can efficiently block the holes and shift hole accumulation zone from the perovskite/ETL interface to the HTL/CsAs interface, resulting in a reduction of the charge accumulation at the recombination zone. In addition, CsAc provides additional Cs sources for transforming $PbBr_2$ into the perovskite phases, resulting in enlarged perovskite grain size and much reduced unreacted $PbBr_2$ defects in the perovskite film. Benefiting from the incorporation of CsAc layer, the as-prepared sky-blue PeLEDs shows considerable improvement of EQE from 5.3 to 9.2%.

2. Results and Discussion

Sky-blue PeLEDs with the structure (**Figure 1a**) of ITO/PEDOT:PSS/PVK/perovskite/POT2T/LiF/Al were fabricated. In the PeLEDs, HTL consists of PEDOT:PSS and Poly(9-vinylcarbazole) (PVK), and ETL is 2,4,6-Tris[3-(diphenylphosphinyl)phenyl]-1,3,5-triazine (POT2T). An energy level diagram of the blue PeLEDs is shown in **Figure 1a**. According to the *J-V* characteristics of the corresponding hole-only devices (HOD) and electron-only devices (EOD) (**Figure S1a, b**), our PeLEDs are hole dominant. **Figure S1b** shows that the hole current of the HOD decreases with increasing concentration of the PVK spin-cast solution which leads to increasing thickness of the PVK films. However, even at 10 mg/mL of PVK, the hole

current of the HOD is still about one order of magnitude higher than the electron current of the EOD, indicating the charge imbalance still exists in the device (**Figure S1b**). However, **Figure S1c** shows that the current density of the PeLED decreases with increasing concentration of PVK. It indicates that the resistance of the PVK layer has influences on the recombination current of the PeLEDs. In fact, the charge transport of the devices significantly depends on the resistance of the responsible layer of minority carrier and the accumulation of major carrier.[36,37] According to the hole-dominated transport properties (**Figure S1b**) and the energy level alignment (**Figure 1a**), it is reasonably considered that the increase of the PVK layer thickness leads to a reduction of hole accumulation inside the PeLEDs, and thus an improvement of EQE (**Figure S1d**) due to a reduced Auger recombination. When the concentration of PVK increases from 5 to 8 mg/mL, the maximum EQE (EQE_{max}) of the PeLEDs increases from 1.6% to 6.8% (**Figure S1d**). However, on the other hand, the reduction of hole accumulation would decrease the potential difference across electron transport region, and thus decrease the carrier injection and transport of the PeLEDs (**Figure S1c**). When the concentration of PVK further increases to 10 mg/mL, the PeLED shows a higher turn-on voltage of 4.2 V and a decreased EQE_{max} of 4.2%.

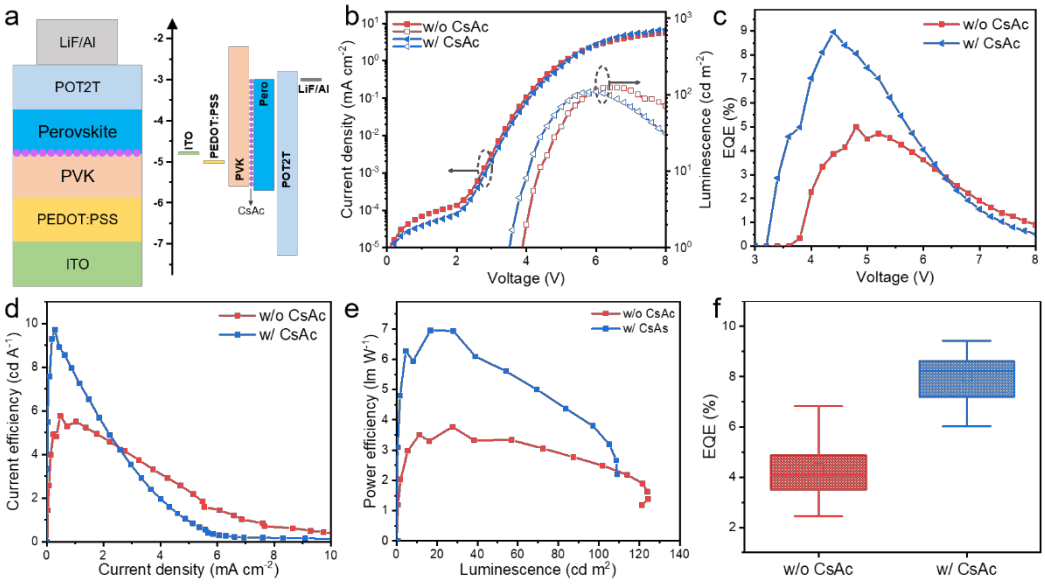

Figure 1. EL performance of PeLEDs without and with CsAc layer. (a) Device structure and energy band alignment diagram. (b) *J-V-L* curves, (c) EQE-*V* curves, (d) *CE-J* curves, (e) *PE-L* curves, and (f) EQE histogram of PeLEDs without and with CsAc layer.

To further improve the performances of the hole-dominated PeLEDs, we inserted an additional CsAc layer between the PVK and the perovskite layers. It has been reported that CsAc shows n-type conductivity.[38] Therefore, holes would be blocked and the charge accumulation zone is expected to shift to the PVK/CsAc interface. To verify our conjecture, we fabricated and compared two PeLEDs with the same device structure, except that one has the additional CsAc layer at the PVK/perovskite interface and the other does not (**Figure 1a**). According to $(ahv)^2$ versus photon energy curves and UPS characterizations, the presence of the CsAc layer has little influence on the energy states of the perovskite film (**Figure S2**). The performance of the PeLED is influenced by changing the concentration of CsAc, and the highest EQE was obtained with the CsAc

concentration of 6 mg/mL (**Figure S3**). **Figure 1b** shows that the current density of the PeLED with the CsAc layer is lower than that of the one without CsAc layer at low driving voltages. When the driving voltage exceeds 3.8 V, the current densities of the devices are nearly the same. This indicates that the CsAc can efficiently block the parasitic current flowing through the whole device, but have little influences on the current density after turning on. The turn-on voltages of the PeLEDs without and with the CsAc layer are respective 4 V and 3.6 V. Their EL intensity increase rapidly after turn-on. The luminance of the PeLED with the CsAc layer is higher than that without the CsAc layer at the same voltage. Thus, the EQE_{max} increases from 5.3% of the PeLED with the CsAs layer to 9.2% of the PeLED with the CsAc layer (**Figure 1c**). A similar trend was obtained for the current efficiency versus current density (*CE-J*) and power efficiency versus L (*PE-L*) characteristics (**Figure 1d, e**), indicating enhanced performance in the PeLED with the CsAc layer. The additional CsAc layer also enhanced the performance reproducibility (**Figure 1f**). The average EQE_{max} of the PeLEDs layer lifts from 4.34% of the device without the CsAc layer to 8.01% for the device with the CsAc layer. The performance improvements of the PeLEDs with CsAc layer are not due to the variation in electroluminescence (EL) spectra (**Figure S4a**). The two devices show sky blue emission with a peak at 486 nm and a full width at half maximum (FWHM) of 21 nm (**Figure S4a**). Angular dependent EL spectra of PeLEDs indicate that the presence of the CsAc layer beneath the perovskite show negligible effect on the angular-dependent EL profile of the PeLED (**Figure S4b, c**). The device with the CsAc layer has good color purity with Commission International de l'Eclairage

(CIE) coordinates of (0.10, 0.23) (**Figure S4d**). The device also exhibits a good EL spectral stability with a negligible peak shift as the driving voltage increases from 3.2 to 4.2 V (left panel of **Figure S4a** and **Figure S4e**). We also tracked the EL spectra during the lifetime test and showed the spectra when the EL intensity decreases from 100 to 10% of its initial value (right panel of **Figure S4a**). Notably, the emission peak position and FWHM show little changes even when the EL intensity drops to 10%. While the insertion of the CsAc layer has little influence on the operational stability of the PeLED (**Figure S4f**).

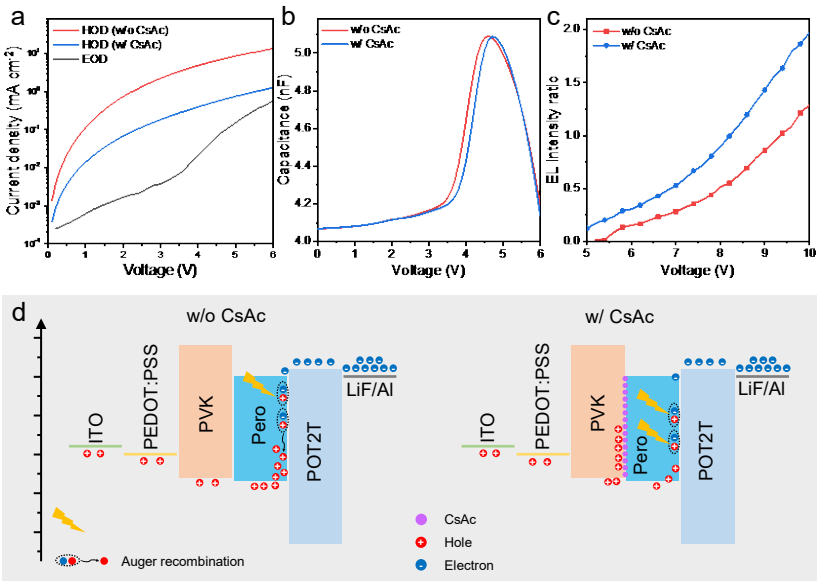

Figure 2. Electronic properties of perovskite devices without and with the CsAc layer. (a) *J-V* relationship of single carrier devices. (b) CV characteristics of devices without and with the CsAc layer. (c) Ratios of EL intensities from blue perovskite and the orange PO-01 for the PeLEDs without and with the CsAc layer. (d) Schematic of energy band alignment and recombination of carriers in PeLEDs without and with CsAc layer, respectively.

We then carried out several electrical measurements to reveal the influences of the CsAc layer on the PeLEDs. *J-V* characteristics of HOD and EOD without and with the CsAc layer are shown in **Figure 2a**. The current density of the HOD with the CsAc layer is one order of magnitude lower than that without the CsAc layer. It suggests that the CsAc layer can efficiently block the hole transport. Nevertheless, comparing to the HOD with the CsAc layer, the current density of the EOD is much lower, indicating that hole current is still dominating in the the PeLED with CsAc. As the CsAc layer has little influence on the current density after turning on (**Figure 1b**), the CsAc layer is reasonably considered to modulate the hole accumulation inside the PeLEDs by its hole blocking effect. Therefore, capacitance-voltage measurements were also conducted to examine the correlation between the carrier accumulation and hole blocking effect in the PeLEDs without and with the CsAc layer. **Figure 2b** shows the capacitance-voltage (CV) characteristic of the devices with and without CsAc. The capacitance of both PeLEDs start to rise sharply at 3.5 V and then decrease at about 4.7 V. When the voltage is over 4.7 V, the recombination process dominates by consuming a large number of the injected carriers, resulting in a rapid decrease in capacitance.[39] On the other hand, over the voltage region from 3.5 to 4.7 V, the space charges dominate the capacitance due to the slow recombination process. The space charges are mainly injected holes in the hole-dominate PeLEDs. Compared to the the PeLED without the CsAc layer, the PeLED with the CsAc layer shows lower capacitance in the region dominated by space charges. This represents the hole accumulation in the device is changed by the CsAc layer. After incorporating the CsAc layer, the hole accumulation is considered to shift

from the the perovskite/ETL interface to the HTL/CsAc interface, leading to a reduction of the capacitance due to a larger distance between the accumulated holes and electrons. It is worth noting that the current density of a working PeLED is determined by the minority carrier.[40] Therefore, the current density shown in **Figure 1b** shows minor difference of PeLEDs without and with CsAc layer after turns on.

We also employed a "probe detection" method to study the influence of carrier accumulation at the perovskite/ETL interface on the devices without and with the CsAc layer. In the "probe detection" experiment, a 0.1 nm orange emitter PO-01 is inserted between the perovskite and POT2T layer as a probe (**Figure S5a, b**).[41] If excitons are formed at the perovskite/ETL interface, energy would transfer to PO-01 and then emit orange light. The EL peak of PO-01 emerge prior to the emission of perovskite (**Figure S5c, d**), indicating the recombination zone is at/near the perovskite/ETL interface. The ratio of emission from perovskite and that from PO-01 can thus represent the exciton distribution at the perovskite/ETL interface. As shown in **Figure 2c**, the ratio of EL emission from perovskite and PO-01 increased gradually with increasing driving voltage for both PeLEDs without and with the CsAc layer. However, the ratio in the PeLED with the CsAc layer is always higher than that without the CsAc layer. It represents that more excitons are formed at/near the perovskite/ETL interface in the PeLEDs with the CsAc layer, resulting in an insufficient energy transfer from perovskite to PO-01. The less excitons of the PeLEDs without the CsAc layer are attributed to more serious Auger recombination due to carrier accumulation at the perovskite/ETL interface. Therefore, as schematically shown in the left panel of **Figure**

2d, in the PeLED without the CsAc layer, hole accumulation at the perovskite/ETL interface, resulting Auger recombination. While hole accumulation is shifted to the PVK/CsAc interface in the PeLED with the CsAc layer (right panel of **Figure 2d**), this can attribute to the more exciton at the perovskite/ETL interface for radiative recombination.

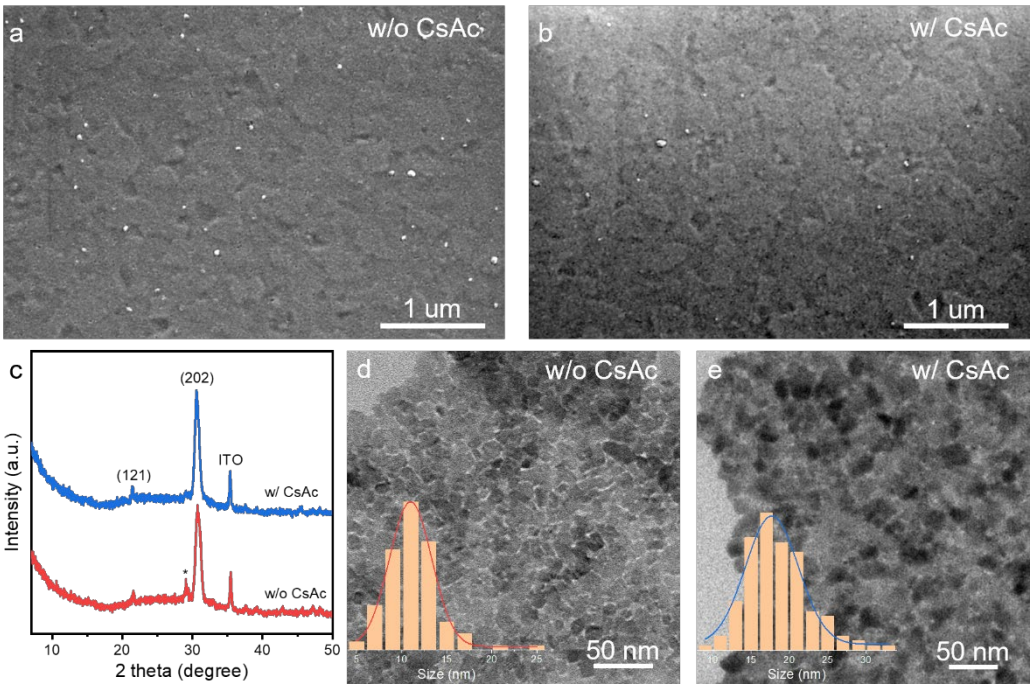

Figure 3. Influences of CsAc layer on the morphologies and structures of perovskite. SEM images of the perovskite films (a) without and (b) with the CsAc layer on PVK. (c) XRD patterns of the perovskite films without and with the CsAc layer. TEM images of the the perovskite (d) without and (e) with the CsAc layer. Inset figures of (d, e) represent the average perovskite crystal grain size in the film without and with the CsAc, respectively.

Apart from the electrical influences of CsAc layer on the carrier dynamics, we conjected that the CsAc layer may also function as surface modifier which can improve

the properties of perovskites as well. Surface modification on the transport layer has been demonstrated being effective to enhance the crystallinity of perovskites and improve the carrier transport capability.[42] Therefore, we also conducted structural and optical investigations on the perovskite film without and without the CsAc layer.

Perovskite films without and with the CsAc layer were prepared by spin-coating precursor solutions containing $PbBr_2$, CsBr, PEACl, and ODEA in DMSO solvent[25,43] on the PVK layer without and with CsAc (**Figure S6a**). Then these films are subjected to thermal annealing to remove residual solvents, leaving bright sky-blue emissive perovskite films (**Figure S6b)**. Contact angle measurement indicates that the CsAc layer has little influence on the wettability of the substrate (**Figure S6c**). We then studied the influences of the CsAc layer on morphologies and structures of the perovskite (**Figure 3**). Morphologies of the perovskite films were characterized using scanning electron microscopy (SEM). An SEM image (**Figure S7**) confirms that the CsAc layer exists as amorphous islands on the PVK layer. For both perovskite films without and with the CsAc layer, they show dense and compact morphology, indicating the CsAc layer shows little influences on the morphology of the perovskite film (**Figure 3a, b**). It is worth noting that some bright dots exist on the surface of perovskite films without the CsAc layer, which can be assigned to the unreacted lead source ($PbBr_2$).[44] In contrast, the number of these bright dots is substantially reduced in the perovskite film without the CsAc layer. This may be attributed to the fact that the CsAc layer provides extra Cs source to interact with $PbBr_2$ to form the perovskite phase, since parts of CsAc can be dissolved in the DMSO solvent.[45] According to the previous report, the

unreacted Pb source on the perovskite film can act as defect sites which is detrimental to the optoelectronic properties of perovskite devices.[44] **Figure 3c** displays X-ray diffraction (XRD) patterns of the perovskite films without and with the CsAc layer. These perovskite films were dominated by the orthorhombic (pnma) crystal structure, consistent with the previous reports.[25,46] Characteristic peaks at 21.4° and 30.6° can be assigned to (121) and (202) crystal planes, respectively.[25,46] The CsAc layer shows little influences on the crystal structure of the perovskite film except for the slight increase of the diffraction peak intensity for the (202) plane of the perovskite (**Figure S8a**). This indicates that incorporating the CsAc layer improves the crystallinity of the perovskite. The diffraction peak at 29.1° belongs to the (201) plane of the unreacted $PbBr_2$ (PDF#31-0679). However, this diffraction peak is largely decreased in the perovskite with the CsAc layer (**Figure S8b**), indicating that CsAc is beneficial to facilitating the formation of three-dimensional (3D) perovskites.[47] It is possible because the CsAc layer on the PVK provides extra Cs source to form perovskite instead of leaving unreacted $PbBr_2$ in the perovskite film. This is constant with the result observed in the SEM image as bright dots representing $PbBr_2$ are reduced (**Figure 3a, b**). Besides, we also measured the transmission electron microscopy (TEM) image of both perovskite films to reveal the influence of the CsAc layer on the crystallinity of perovskites. As shown in **Figure 3d**, the crystal with an average grain size of 11.2 nm in the perovskite film without the CsAc layer can be assigned to the 3D perovskite. After introducing the CsAc layer on the PVK, the perovskite grain size increases to give an average grain size of 18.6 nm (**Figure 3e**). As shown in the high-resolution transmission electron

microscopy (HRTEM) images (**Figure S9a, b**), the lattice fringe of 0.29 nm can be assigned to the (202) plane of 3D perovskite crystals,[48] corresponding to the diffraction peak at 30.6° in XRD patterns. The increased grain size in the perovskite film with the CsAc layer indicates that the crystallinity of the perovskite film is improved, which is in line with the XRD results. As shown in the selected area electron diffraction (SAED) patterns (**Figure S9c, d**), the perovskite nanocrystals without and with the CsAc layer are both polycrystalline. In comparison, the much sharper diffraction rings indicate the enhanced crystallinity of the perovskite with the CsAc modification compared to that without the CsAc modification (**Figure S9c, d**). This further confirm the crystallinity improvement of perovskite film on the CsAc modified PVK layer. Therefore, we can conclude that the CsAc modification on the PVK layer is beneficial to the growth of the perovskite film.

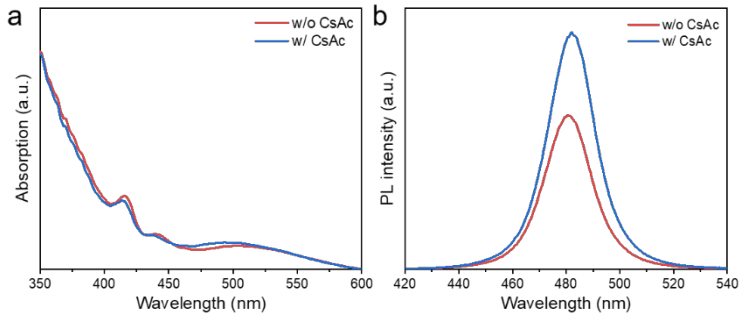

Figure 4. Optical properties of perovskites without and with CsAc layer. (a) Absorbance, (b) PL spectra of perovskite films without and with CsAc layer.

Finally, we studied the optical properties of the perovskite films without and with the CsAc layer **(Figure 4)**. Absorption spectra of the perovskite films are shown in **Figure 4a**. A distinct excitonic peak at 414 nm appears, corresponding to n = 2 phase,

implying that a low-dimensional phase exists in the perovskite film. The broad absorption peak at about 500 nm is ascribed to PVK and perovskite with higher "n" value phases. With the addition of the CsAc layer beneath the perovskite layer, the absorption peak intensity at 414 nm is slightly decreased. Meanwhile, the intensity of the absorption peak of higher dimensional perovskite is increased. This suggests that the CsAc layer inhibits the formation of low dimensional perovskite while facilitating the formation of higher dimensional perovskite phases. The perovskite films without and with the CsAc layer emit sky-blue light with emission peaks at 480 and 482 nm, respectively (**Figure 4b**). The perovskite films without the CsAc layer show weaker PL intensities, which may be attributed to exciton quenching caused by the charge transfer at the PVK–perovskite interface.[49] Moreover, as revealed in the XRD results (**Figure 3c**), the slight improvement of the crystallinity of perovskite film can also benefit the reduced defects in the perovskite, resulting in enhanced PL intensity of the perovskite film with the CsAc layer. No emission peak at shorter wavelength, belonging to the quasi-two-dimensional (quasi-2D) perovskite, can be found in the PL spectra for both perovskite films (**Figure S10a**). This may result from the efficient energy transfer from low "n" value to high "n" value domains. Time-resolved photoluminescence lifetime (TRPL) result shows that the lifetime exhibits slight prolongation in the perovskite film with the CsAc layer of 91 ns compared to that of 89 ns in perovskite film without the CsAc layer (**Figure S10b**). Similar to the improvement in the PL intensity, both inhibit charge transfer loss and suppression of non-radiative energy loss could contribute to the increment of PL lifetime. These improvement in the optical properties of perovskites

contribute to the EQE increase in the PeLEDs with the CsAc layer.

3. Conclusions

In summary, we demonstrate that introducing an additional CsAc layer on the surface of HTL can further improve the performance of PeLEDs. The hole accumulation at the perovskite/ETL interface is alleviated due to a shift of the accumulation zone to the HTL/CsAc interface. Separation between carrier accumulation zone and exciton recombination zone substantially suppress the Auger recombination, leading to an improvement of radiative efficiency. Moreover, the crystallinity of the perovskite film with CsAc layer is slightly improved which favors suppressed non-radiative loss. As a result, benefiting from the conducive effect of CsAc, the EQE of the corresponding PeLEDs improved from 5.3 to 9.2%.

4. Experimental section

Materials: $PbBr_2$ (99.99%), PEACl (> 99.5%) and PVK (Mn > 100000) were purchased from Xi'an Polymer Light Technology Corp. CsBr (99.999%), CsAc (99.999%), ODEA (98%), PFI (5 wt.% in lower aliphatic alcohols and water, contains 15–20% water), dimethyl sulfoxide (DMSO, 99.9%, anhydrous), chlorobenzene (CB, 99.8%, anhydrous) and 2-propanool (IPA, 99.5%, anhydrous) were purchased from Sigma-Aldrich. PEDOT:PSS, LiF and POT2T, PO-01 were purchased from Lumtec. All chemicals were used as purchased.

Preparation of precursor solutions: $PbBr_2$ (23 mg), CsBr (18 mg) and PEACl (10 mg) were added into 1 mL of DMSO as precursor solution. Diluted ODEA solution was

prepared by dissolving 20 μL of ODEA into 1 mL DMSO. 25 μL of diluted ODEA solution was added into the perovskite precursor solution as passivation agent. The precursor solution was stirred overnight before use. PVK solution was prepared by dissolving PVK (5-10 mg/mL) in CB and was stirred for 12 hours before use. CsAc solution was prepared by dissolving CsAc in IPA.

Preparation of perovskite films: The ITO and quartz substrates are treated with UV-ozone. PVK layer was spin-coated on the substrate, followed by thermal annealing at 130 °C for 20 min to remove residual CB solvent. To prepare perovskite film with CsAc layer, CsAc solution in IPA was spin coated onto PVK film. Subsequently, perovskite precursor solution was spin-coated on the substrate. The preparation of perovskite film without CsAc layer is similar to that with CsAc layer except the CsAc solution is substitute with IPA alone. The substrates are then annealed at 70 °C for 10 min to remove excessive DMSO solvent.

Characterization of perovskite films: Absorption spectra were recorded using a Shimadzu 1700 model UV-vis spectrometer. Steady-state and time-resolved PL spectra were recorded with an FLS 980 spectrofluorometer (Edinburgh Instruments Ltd.). A 375 nm laser is used as an excitation source in time-resolved measurement. X-ray diffraction patterns were recorded with a D2 Phaser instrument with Cu Kα (λ = 0.154056 nm) radiation. Scanning electron microscopy (SEM) images were taken with a Thermo Fisher scanning electron microscope Quattro-s FEG. TEM and HRTEM were conducted with a JEOL JEM-2011Plus at 200 kV. The perovskite film was peeled from the substrate by sonicating the substrate in toluene solution. Then the solution was

dropped onto the copper grid for further TEM and HRTEM characterizations.

Fabrication of PeLEDs: The PeLEDs were fabricated with the device structure of ITO/PEDOT:PSS/PVK(with or without CsAc)/perovskite/POT2T/LiF/Al. Indium tin oxide (ITO)-coated glasses were cleaned using Decon 90 detergent and washed sequentially with deionized water, acetone and ethanol. Cleaned ITO glasses were dried in an oven overnight. Before use, ITO glasses were treated with UV ozone (UVO) for 20 min. PEDOT:PSS was spin-coated onto ITO glasses and dried at 140 °C to remove water. The substrates were then transferred into an N_2-filled glovebox. The PVK precursor was spin-coated on the substrate at 3000 rpm for 60 s followed by annealing at 130 °C for 20 min. After that, CsAc solution in IPA was spin-coated on PVK. The perovskite precursor solution was then spin-coated at a speed of 3000 rpm and annealed at 70 °C for 8 min. Then the as-prepared perovskite films were transferred to high-vacuum deposition system. POT2T (45 nm), LiF (1 nm) and Al (100 nm) cathode were deposited sequentially under a pressure of 1×10^{-6} Torr. After cooling down for 30 min, the device was encapsulated with a glass lid and epoxy resin in a glovebox.

Fabrication of single-carrier devices: HOD were fabricated with the device structure of ITO/PEDOT:PSS/PVK (with or without CsAc)/perovskite/TFB/MoO_3/Ag. PEDOT:PSS, PVK, CsAc, perovskite precursor and TFB (8 mg/mL at 3000 rpm for 60 s) were spin-coated sequentially. Then the perovskite films were transferred to the high-vacuum deposition system to successively evaporate MoO_3 (10 nm) and Ag (100 nm). EOD were fabricated with the device structure of ITO/C_{60}/perovskite/POT2T/LiF/Al. C_{60} (10 nm) was evaporated onto the ITO substrates first in the high-vacuum deposition

system. Then, the substrates were transferred to the glove box, and perovskite precursor solution were spin-coated. Finally, the substrates were transferred to the high-vacuum deposition system for the evaporation of POT2T (45 nm), LiF (1 nm) and Al (100 nm). After cooling down for 30 min, the device was encapsulated with a glass lid and epoxy resin in a glovebox.

Characterization of perovskite devices:

The device area is 0.1 cm^2. EL spectra and luminescence were measured with a PMA-12 photonic multichannel analyzer (Hamamatsu). J-L-V relationship were recorded using a computer-controlled Keithley 2400 source meter.

ASSOCIATED CONTENT

Supporting Information.

The Supporting Information is available free of charge at

EL characterization on PeLEDs based on different concentration of PVK and CsAc; spectral and operational stability of PeLEDs; angular dependent EL spectra of PeLEDs; energy level characterizations of perovskite; EL spectra of "probe detection" devices; photographs of perovskite films; contact angle characterizations; SEM images of PVK layer and CsAc on PVK layer; XRD patterns of perovskite films; TEM image and SAED patterns of perovskites; PL spectra and PL lifetime of perovskite films.

AUTHOR INFORMATION

Corresponding Author

Shihao Liu – Center of Super-Diamond and Advanced Films (COSDAF) and Department of Chemistry, City University of Hong Kong, Hong Kong SAR 999077, P. R. China; Email: liushihao@jlu.edu.cn

Xiao Huang – Institute of Advanced Materials (IAM), Nanjing Tech University, 30 South Puzhu Road, Nanjing, 211816 P. R. China; Email: iamxhuang@njtech.edu.cn

Chun-Sing Lee – Center of Super-Diamond and Advanced Films (COSDAF) and Department of Chemistry, City University of Hong Kong, Hong Kong SAR 999077, P. R. China; Email: apcslee@cityu.edu.hk

Authors

Zhaohua Zhu – Center of Super-Diamond and Advanced Films (COSDAF) and Department of Chemistry, City University of Hong Kong, Hong Kong SAR 999077, P. R. China

Yang Li – Center of Super-Diamond and Advanced Films (COSDAF) and Department of Chemistry, City University of Hong Kong, Hong Kong SAR 999077, P. R. China

Zhiqiang Guan – Center of Super-Diamond and Advanced Films (COSDAF) and Department of Chemistry, City University of Hong Kong, Hong Kong SAR 999077, P. R. China

Yan Wu – Center of Super-Diamond and Advanced Films (COSDAF) and Department of Chemistry, City University of Hong Kong, Hong Kong SAR 999077, P. R. China

Zixin Zeng – Center of Super-Diamond and Advanced Films (COSDAF) and Department of Material Science and Engineering, City University of Hong Kong, Kowloon 999077, Hong Kong SAR, P. R. China

Sai-Wing Tsang – Center of Super-Diamond and Advanced Films (COSDAF) and Department of Material Science and Engineering, City University of Hong Kong, Kowloon 999077, Hong Kong SAR, P. R. China

Author Contributions

The manuscript was written through the contributions of all authors. All authors have approved the final version of the manuscript.

Notes

The authors declare no competing financial interest.

ACKNOWLEDGMENT

This work was supported by the Research Grants Council of the Hong Kong Special Administrative Region, China (11300418).

Reference

(1) Kovalenko, M. V.; Protesescu, L.; Bodnarchuk, M. I. Properties and Potential Optoelectronic Applications of Lead Halide Perovskite Nanocrystals. *Science* **2017**, *358* (6364), 745-750.
(2) Cho, H.; Jeong, S. H.; Park, M. H.; Kim, Y. H.; Wolf, C.; Lee, C. L.; Heo, J. H.; Sadhanala, A.; Myoung, N.; Yoo, S.; Im, S. H.; Friend, R. H.; Lee, T. W. Overcoming the Electroluminescence Efficiency Limitations of Perovskite Light-Emitting Diodes. *Science* **2015**, *350* (6265), 1222-1225.
(3) Xiao, Z. G.; Kerner, R. A.; Zhao, L. F.; Tran, N. L.; Lee, K. M.; Koh, T. W.; Scholes, G. D.; Rand, B. P. Efficient Perovskite Light-Emitting Diodes Featuring Nanometre-Sized Crystallites. *Nat. Photonics* **2017**, *11* (2), 108-115.

(4) Yuan, M.; Quan, L. N.; Comin, R.; Walters, G.; Sabatini, R.; Voznyy, O.; Hoogland, S.; Zhao, Y.; Beauregard, E. M.; Kanjanaboos, P.; Lu, Z.; Kim, D. H.; Sargent, E. H. Perovskite Energy Funnels for Efficient Light-Emitting Diodes. *Nat. Nanotechnol.* **2016**, *11* (10), 872-877.
(5) Stranks, S. D.; Snaith, H. J. Metal-Halide Perovskites for Photovoltaic and Light-Emitting Devices. *Nat. Nanotechnol.* **2015**, *10* (5), 391-402.
(6) Yang, X.; Zhang, X.; Deng, J.; Chu, Z.; Jiang, Q.; Meng, J.; Wang, P.; Zhang, L.; Yin, Z.; You, J. Efficient Green Light-Emitting Diodes Based on Quasi-Two-Dimensional Composition and Phase Engineered Perovskite with Surface Passivation. *Nat. Commun.* **2018**, *9* (1), 570.
(7) Akkerman, Q. A.; D'Innocenzo, V.; Accornero, S.; Scarpellini, A.; Petrozza, A.; Prato, M.; Manna, L. Tuning the Optical Properties of Cesium Lead Halide Perovskite Nanocrystals by Anion Exchange Reactions. *J. Am. Chem. Soc.* **2015**, *137* (32), 10276-10281.
(8) Zhu, Z.; Zeng, S.; Chen, Q.; Yang, L.; Wei, C.; Chen, B.; Yu, H.; Li, H.; Zhang, J.; Huang, X. One-step synthesis of epitaxial 3D/2D metal halide perovskite heterostructures. *Chem. Commun.* **2022**.
(9) Zhu, Z.; Zhu, C.; Yang, L.; Chen, Q.; Zhang, L.; Dai, J.; Cao, J.; Zeng, S.; Wang, Z.; Wang, Z.; Zhang, W.; Bao, J.; Yang, L.; Yang, Y.; Chen, B.; Yin, C.; Chen, H.; Cao, Y.; Gu, H.; Yan, J.; Wang, N.; Xing, G.; Li, H.; Wang, X.; Li, S.; Liu, Z.; Zhang, H.; Wang, L.; Huang, X.; Huang, W. Room-temperature epitaxial welding of 3D and 2D perovskites. *Nat. Mater.* **2022**, *21* (9), 1042-1049.
(10) Teng, P. P.; Reichert, S.; Xu, W. D.; Yang, S. C.; Fu, F.; Zou, Y. T.; Yin, C. Y.; Bao, C. X.; Karlsson, M.; Liu, X. J.; Qin, J. J.; Yu, T.; Tress, W.; Yang, Y.; Sun, B. Q.; Deibel, C.; Gao, F. Degradation and Self-Repairing in Perovskite Light-Emitting Diodes. *Matter* **2021**, *4* (11), 3710-3724.
(11) Zhu, L.; Cao, H.; Xue, C.; Zhang, H.; Qin, M.; Wang, J.; Wen, K.; Fu, Z.; Jiang, T.; Xu, L.; Zhang, Y.; Cao, Y.; Tu, C.; Zhang, J.; Liu, D.; Zhang, G.; Kong, D.; Fan, N.; Li, G.; Yi, C.; Peng, Q.; Chang, J.; Lu, X.; Wang, N.; Huang, W.; Wang, J. Unveiling the Additive-Assisted Oriented Growth of Perovskite Crystallite for High Performance Light-Emitting Diodes. *Nat. Commun.* **2021**, *12* (1), 5081.
(12) Ma, D.; Lin, K.; Dong, Y.; Choubisa, H.; Proppe, A. H.; Wu, D.; Wang, Y. K.; Chen, B.; Li, P.; Fan, J. Z.; Yuan, F.; Johnston, A.; Liu, Y.; Kang, Y.; Lu, Z. H.; Wei, Z.; Sargent, E. H. Distribution Control Enables Efficient Reduced-Dimensional Perovskite LEDs. *Nature* **2021**, *599* (7886), 594-598.
(13) Chu, Z.; Ye, Q.; Zhao, Y.; Ma, F.; Yin, Z.; Zhang, X.; You, J. Perovskite Light-Emitting Diodes with External Quantum Efficiency Exceeding 22% via Small-Molecule Passivation. *Adv. Mater.* **2021**, *33* (18), e2007169.
(14) Chu, Z.; Zhao, Y.; Ma, F.; Zhang, C. X.; Deng, H.; Gao, F.; Ye, Q.; Meng, J.; Yin, Z.; Zhang, X.; You, J. Large Cation Ethylammonium Incorporated Perovskite for Efficient and Spectra Stable Blue Light-Emitting Diodes. *Nat. Commun.* **2020**, *11* (1), 4165.
(15) Lin, K.; Xing, J.; Quan, L. N.; de Arquer, F. P. G.; Gong, X.; Lu, J.; Xie, L.; Zhao, W.; Zhang, D.; Yan, C.; Li, W.; Liu, X.; Lu, Y.; Kirman, J.; Sargent, E. H.; Xiong, Q.;

Wei, Z. Perovskite Light-Emitting Diodes with External Quantum Efficiency Exceeding 20 Per Cent. *Nature* **2018**, *562* (7726), 245-248.
(16) Cao, Y.; Wang, N.; Tian, H.; Guo, J.; Wei, Y.; Chen, H.; Miao, Y.; Zou, W.; Pan, K.; He, Y.; Cao, H.; Ke, Y.; Xu, M.; Wang, Y.; Yang, M.; Du, K.; Fu, Z.; Kong, D.; Dai, D.; Jin, Y.; Li, G.; Li, H.; Peng, Q.; Wang, J.; Huang, W. Perovskite Light-Emitting Diodes Based on Spontaneously Formed Submicrometre-Scale Structures. *Nature* **2018**, *562* (7726), 249-253.
(17) Wang, Q.; Wang, X.; Yang, Z.; Zhou, N.; Deng, Y.; Zhao, J.; Xiao, X.; Rudd, P.; Moran, A.; Yan, Y.; Huang, J. Efficient Sky-Blue Perovskite Light-Emitting Diodes via Photoluminescence Enhancement. *Nat. Commun.* **2019**, *10* (1), 5633.
(18) Pang, P.; Jin, G.; Liang, C.; Wang, B.; Xiang, W.; Zhang, D.; Xu, J.; Hong, W.; Xiao, Z.; Wang, L.; Xing, G.; Chen, J.; Ma, D. Rearranging Low-Dimensional Phase Distribution of Quasi-2D Perovskites for Efficient Sky-Blue Perovskite Light-Emitting Diodes. *ACS Nano* **2020**, *14* (9), 11420-11430.
(19) Zhu, Z. H.; Wu, Y.; Shen, Y.; Tan, J. H.; Shen, D.; Lo, M. F.; Li, M. L.; Yuan, Y.; Tang, J. X.; Zhang, W. J.; Tsang, S. W.; Guan, Z. Q.; Lee, C. S. Highly Efficient Sky-Blue Perovskite Light-Emitting Diode Via Suppressing Nonradiative Energy Loss. *Chem. Mater.* **2021**, *33* (11), 4154-4162.
(20) Zhu, Z.; Wu, Y.; Li, Y.; Zeng, Z.; Tsang, S.-W.; Guan, Z.; Lee, C.-S. Enhancing the Performance of Perovskite Light-Emitting Diodes by Humidity Treatment. *ACS Appl. Mater. Interfaces* **2022**, *14* (17), 19774-19784.
(21) Gunnarsson, W. B.; Xu, Z.; Noel, N. K.; Rand, B. P. Improved Charge Balance in Green Perovskite Light-Emitting Diodes with Atomic-Layer-Deposited Al_2O_3. *ACS Appl. Mater. Interfaces* **2022**, *14* (30), 34247-34252.
(22) Jin, X.; Chang, C.; Zhao, W.; Huang, S.; Gu, X.; Zhang, Q.; Li, F.; Zhang, Y.; Li, Q. Balancing the Electron and Hole Transfer for Efficient Quantum Dot Light-Emitting Diodes by Employing a Versatile Organic Electron-Blocking Layer. *ACS Appl. Mater. Interfaces* **2018**, *10* (18), 15803-15811.
(23) Li, Z.; Chen, Z.; Yang, Y.; Xue, Q.; Yip, H.-L.; Cao, Y. Modulation of recombination zone position for quasi-two-dimensional blue perovskite light-emitting diodes with efficiency exceeding 5%. *Nat. Commun.* **2019**, *10* (1), 1027.
(24) Zhai, Y.; Wang, K.; Zhang, F.; Xiao, C.; Rose, A. H.; Zhu, K.; Beard, M. C. Individual Electron and Hole Mobilities in Lead-Halide Perovskites Revealed by Noncontact Methods. *ACS Energy Lett.* **2020**, *5* (1), 47-55.
(25) Guan, Z.; Li, Y.; Zhu, Z.; Zeng, Z.; Shen, D.; Tan, J.; Tsang, S.-W.; Liu, S.; Lee, C.-S. Efficient Perovskite White Light-Emitting Diode Based on an Interfacial Charge-Confinement Structure. *ACS Appl. Mater. Interfaces* **2021**, *13* (37), 44991-45000.
(26) Zhang, L.; Yang, X.; Jiang, Q.; Wang, P.; Yin, Z.; Zhang, X.; Tan, H.; Yang, Y.; Wei, M.; Sutherland, B. R.; Sargent, E. H.; You, J. Ultra-bright and highly efficient inorganic based perovskite light-emitting diodes. *Nat. Commun.* **2017**, *8* (1), 15640.
(27) Wang, N.; Cheng, L.; Ge, R.; Zhang, S.; Miao, Y.; Zou, W.; Yi, C.; Sun, Y.; Cao, Y.; Yang, R.; Wei, Y.; Guo, Q.; Ke, Y.; Yu, M.; Jin, Y.; Liu, Y.; Ding, Q.; Di, D.; Yang, L.; Xing, G.; Tian, H.; Jin, C.; Gao, F.; Friend, R. H.; Wang, J.; Huang, W. Perovskite light-emitting diodes based on solution-processed self-organized multiple quantum

wells. *Nat. Photonics* **2016**, *10* (11), 699-704.
(28) Li, Z.; Cao, K.; Li, J.; Du, X.; Tang, Y.; Yu, B. Modification of interface between PEDOT:PSS and perovskite film inserting an ultrathin LiF layer for enhancing efficiency of perovskite light-emitting diodes. *Org. Electron.* **2020**, *81*, 105675.
(29) Shen, Y.; Wu, H.-Y.; Li, Y.-Q.; Shen, K.-C.; Gao, X.; Song, F.; Tang, J.-X. Interfacial Nucleation Seeding for Electroluminescent Manipulation in Blue Perovskite Light-Emitting Diodes. *Adv. Funct. Mater.* **2021**, *31* (45), 2103870.
(30) Shen, Y.; Li, Y.-Q.; Zhang, K.; Zhang, L.-J.; Xie, F.-M.; Chen, L.; Cai, X.-Y.; Lu, Y.; Ren, H.; Gao, X.; Xie, H.; Mao, H.; Kera, S.; Tang, J.-X. Multifunctional Crystal Regulation Enables Efficient and Stable Sky-Blue Perovskite Light-Emitting Diodes. *Adv. Funct. Mater.* **2022**, 2206574.
(31) Chen, Z.; Li, Z.; Hopper, T. R.; Bakulin, A. A.; Yip, H.-L. Materials, photophysics and device engineering of perovskite light-emitting diodes. *Rep. Prog. Phys.* **2021**, *84* (4), 046401.
(32) Yang, F.; Chen, H.; Zhang, R.; Liu, X.; Zhang, W.; Zhang, J.; Gao, F.; Wang, L. Efficient and Spectrally Stable Blue Perovskite Light-Emitting Diodes Based on Potassium Passivated Nanocrystals. *Adv. Funct. Mater.* **2020**, *30* (10), 1908760.
(33) Ochsenbein, S. T.; Krieg, F.; Shynkarenko, Y.; Rainò, G.; Kovalenko, M. V. Engineering Color-Stable Blue Light-Emitting Diodes with Lead Halide Perovskite Nanocrystals. *ACS Appl. Mater. Interfaces* **2019**, *11* (24), 21655-21660.
(34) Wang, R.; Zhang, Y.; Yu, F.-X.; Dong, Y.; Jia, Y.-L.; Ma, X.-J.; Xu, Q.; Deng, Y.; Xiong, Z.-H.; Gao, C.-H. An efficient $CsPbBr_3$ perovskite light-emitting diode by employing 1,3,5-tri(m-pyrid-3-yl-phenyl)benzene as a hole and exciton blocking layer. *J. Lumines.* **2020**, *219*, 116915.
(35) Yoon, E.; Jang, K. Y.; Park, J.; Lee, T.-W. Understanding the Synergistic Effect of Device Architecture Design toward Efficient Perovskite Light-Emitting Diodes Using Interfacial Layer Engineering. *Adv. Mater. Interfaces* **2021**, *8* (3), 2001712.
(36) Noguchi, Y.; Hofmann, A.; Brütting, W. Controlling Charge Accumulation Properties of Organic Light-Emitting Diodes using Dipolar Doping of Hole Transport Layers. *Adv. Opt. Mater.* **2022**, *10* (21), 2201278.
(37) Liu, S.; Zhang, J.; Zang, C.; Zhang, L.; Xie, W.; Lee, C.-S. Centimeter-scale hole diffusion and its application in organic light-emitting diodes. *Sci. Adv.* **2022**, *8* (17), eabm1999.
(38) Arafat Mahmud, M.; Kumar Elumalai, N.; Baishakhi Upama, M.; Wang, D.; Gonçales, V. R.; Wright, M.; Justin Gooding, J.; Haque, F.; Xu, C.; Uddin, A. Cesium compounds as interface modifiers for stable and efficient perovskite solar cells. *Sol. Energy Mater. Sol. Cells* **2018**, *174*, 172-186.
(39) Zhang, L.; Nakanotani, H.; Adachi, C. Capacitance-voltage characteristics of a 4,4′-bis[(N-carbazole)styryl]biphenyl based organic light-emitting diode: Implications for characteristic times and their distribution. *Appl. Phys. Lett.* **2013**, *103* (9), 093301.
(40) Khan, R.; Chu, S.; Li, Z.; Ighodalo, K. O.; Chen, W.; Xiao, Z. High Radiance of Perovskite Light-Emitting Diodes Enabled by Perovskite Heterojunctions. *Adv. Funct. Mater.* **2022**, *32* (32), 2203650.

(41) Liu, S.; Zang, C.; Zhang, J.; Tian, S.; Wu, Y.; Shen, D.; Zhang, L.; Xie, W.; Lee, C.-S. Air-Stable Ultrabright Inverted Organic Light-Emitting Devices with Metal Ion-Chelated Polymer Injection Layer. *Nano-Micro Lett.* **2021**, *14* (1), 14.
(42) Shen, Y.; Wang, J.-K.; Li, Y.-Q.; Shen, K.-C.; Su, Z.-H.; Chen, L.; Guo, M.-L.; Cai, X.-Y.; Xie, F.-M.; Qian, X.-Y.; Gao, X.; Zhidkov, I. S.; Tang, J.-X. Interfacial "Anchoring Effect" Enables Efficient Large-Area Sky-Blue Perovskite Light-Emitting Diodes. *Adv. Sci.* **2021**, *8* (19), 2102213.
(43) Xu, W.; Hu, Q.; Bai, S.; Bao, C.; Miao, Y.; Yuan, Z.; Borzda, T.; Barker, A. J.; Tyukalova, E.; Hu, Z.; Kawecki, M.; Wang, H.; Yan, Z.; Liu, X.; Shi, X.; Uvdal, K.; Fahlman, M.; Zhang, W.; Duchamp, M.; Liu, J.-M.; Petrozza, A.; Wang, J.; Liu, L.-M.; Huang, W.; Gao, F. Rational molecular passivation for high-performance perovskite light-emitting diodes. *Nat. Photonics* **2019**, *13* (6), 418-424.
(44) Zhao, L.; Li, Q.; Hou, C.-H.; Li, S.; Yang, X.; Wu, J.; Zhang, S.; Hu, Q.; Wang, Y.; Zhang, Y.; Jiang, Y.; Jia, S.; Shyue, J.-J.; Russell, T. P.; Gong, Q.; Hu, X.; Zhu, R. Chemical Polishing of Perovskite Surface Enhances Photovoltaic Performances. *J. Am. Chem. Soc.* **2022**, *144* (4), 1700-1708.
(45) Guan, Z.; Li, Y.; Zhu, Z.; Zeng, Z.; Chen, Z.; Ren, Z.; Li, G.; Tsang, S.-W.; Yip, H.-L.; Xiong, Y.; Lee, C.-S. High-Efficiency Blue Perovskite Light-Emitting Diodes with Improved Photoluminescence Quantum Yield via Reducing Trap-Induced Recombination and Exciton–Exciton Annihilation. *Adv. Funct. Mater.* **2022**, 2203962.
(46) Cheng, L. P.; Huang, J. S.; Shen, Y.; Li, G. P.; Liu, X. K.; Li, W.; Wang, Y. H.; Li, Y. Q.; Jiang, Y.; Gao, F.; Lee, C. S.; Tang, J. X. Efficient $CsPbBr_3$ Perovskite Light-Emitting Diodes Enabled by Synergetic Morphology Control. *Adv. Opt. Mater.* **2019**, *7* (4), 1801534.
(47) Jena, A. K.; Ishii, A.; Guo, Z.; Kamarudin, M. A.; Hayase, S.; Miyasaka, T. Cesium Acetate-Induced Interfacial Compositional Change and Graded Band Level in $MAPbI_3$ Perovskite Solar Cells. *ACS Appl. Mater. Interfaces* **2020**, *12* (30), 33631-33637.
(48) Cai, Y.; Zhang, P.; Bai, W.; Lu, L.; Wang, L.; Chen, X.; Xie, R.-J. Synthesizing Bright $CsPbBr_3$ Perovskite Nanocrystals with High Purification Yields and Their Composites with In Situ-Polymerized Styrene for Light-Emitting Diode Applications. *ACS Sustain. Chem. Eng.* **2022**, *10* (22), 7385-7393.
(49) Wang, H.; Yuan, H.; Yu, J.; Zhang, C.; Li, K.; You, M.; Li, W.; Shao, J.; Wei, J.; Zhang, X.; Chen, R.; Yang, X.; Zhao, W. Boosting the Efficiency of NiO_x-Based Perovskite Light-Emitting Diodes by Interface Engineering. *ACS Appl. Mater. Interfaces* **2020**, *12* (47), 53528-53536.

Table of Contents Graphic